A Vertical Equilibrium Model for CO_2 Migration in Depleted Gas Fields

Saeid Telvari[1,*], Hariharan Ramachandran[1], Gang Wang[1], Florian Doster[1]

[1]Institute of GeoEnergy Engineering (IGE), School of Energy, Geoscience, Infrastructure and Society, Heriot-Watt University, Edinburgh, EH14 4AS, UK

[*]Corresponding author: Saeid Telvari (st4014@hw.ac.uk)

Preprint statement.

This manuscript is a non-peer-reviewed preprint submitted to **EarthArXiv**. The manuscript has also been submitted to *Water Resources Research* for peer review. Subsequent versions of this preprint may differ in content following peer review; if accepted, the final version will be available via a *DOI* link on this preprint page. Please feel free to contact any of the authors with feedback.

ORCID: https://orcid.org/0000-0002-4896-295X

Keywords: Vertical equilibrium modeling; CO_2 storage; Depleted gas reservoirs; Reservoir simulation.

A Vertical Equilibrium Model for CO_2 Migration in Depleted Gas Fields

Saeid Telvari[1,*], Hariharan Ramachandran[1], Gang Wang[1], and Florian Doster[1]

[1]Institute of GeoEnergy Engineering (IGE), School of Energy, Geoscience, Infrastructure and Society, Heriot-Watt University, Edinburgh, EH14 4AS, UK

[*]Corresponding author: st4014@hw.ac.uk

Abstract

This study presents an extension of the vertical equilibrium (VE) modeling framework to simulate multi-phase flow involving CO_2, methane, and brine in depleted gas reservoirs. The primary motivation is to enable efficient and accurate simulation of CO_2 injection and migration in situations where methane is present, which introduces additional complexity not captured in traditional VE models. The proposed model integrates a black-oil approximation with VE assumptions, reducing the dimensionality of the problem and allowing for rapid simulation of large-scale CO_2 injection in depleted gas reservoirs. By representing CO_2 and methane as separate compressible phases, and treating brine as an incompressible phase, the model achieves a balance between computational speed and physical realism. Pressure-dependent density and viscosity relationships for CO_2 and methane enable accurate thermophysical property estimation without computationally intensive flash calculations. Three case studies validate the model: (1) a flat, layered reservoir benchmark demonstrating accurate CO_2 plume behavior under buoyancy control; (2) a dual-anticline scenario showing that the VE model reproduces the large-scale plume geometry and inter-anticline mass redistribution observed in compositional simulations; and (3) a field-scale application to the Hugin Formation East, where the VE model replicates key features of CO_2 and methane migration observed in compositional models. In all cases, the VE model runs orders of magnitude faster than full 3D simulations while capturing large-scale displacement dynamics effectively. Although the present formulation neglects some physics such as explicit mixing, dissolution, and capillary fringe effects, it still captures the first order displacement behaviour while offering up to 100× speedups. This makes the model a practical tool for rapid screening, uncertainty quantification, and optimisation workflows in CCS projects targeting depleted gas reservoirs.

This study extends the vertical equilibrium (VE) modeling framework to simulate multi-phase flow involving CO_2, methane, and brine in depleted gas reservoirs. Methane presence introduces complexity not captured in traditional VE models. The proposed model integrates a black-oil approximation with VE assumptions, reducing dimensionality and enabling rapid simulation of large-scale CO_2 injection. By representing CO_2 and methane as separate compressible phases, and treating brine as incompressible, the model balances computational speed and physical realism. Pressure-dependent density and viscosity relationships for CO_2 and methane enable accurate property estimation without flash calculations. Three case studies validate the model: (1) a flat, layered reservoir benchmark demonstrating accurate CO_2 plume behavior under buoyancy control; (2) a dual-anticline scenario demonstrating that the VE model reproduces the large-scale plume geometry and inter-anticline mass redistribution observed in compositional simulations; and (3) a field-scale application to the Hugin Formation East, where the VE model replicates key features of CO_2 and methane migration observed in compositional models. The VE model runs orders of magnitude faster than full 3D simulations while capturing large-scale displacement dynamics. Although the formulation neglects explicit mixing, dissolution, and capillary fringe effects, it captures first-order displacement behaviour with speedups up to 100×. This makes it a practical

tool for screening, uncertainty quantification, and optimisation in CCS projects targeting depleted gas reservoirs.

Plain Language Summary

Storing carbon dioxide (CO_2) underground in depleted gas reservoirs is a promising way to reduce greenhouse gas emissions. However, predicting how injected CO_2 moves in these reservoirs is difficult because the pore space may still contain natural gas and water, and detailed computer models can be very slow. In this study, we developed a faster modeling approach to simulate how CO_2, methane, and brine move together after CO_2 injection. The method is based on the idea that fluids can quickly arrange themselves vertically under gravity, which allows the model to simplify the problem while still capturing the main large-scale behavior. We tested the method in three cases, from simple idealized settings to a field-scale reservoir model. The results show that the new model reproduces the main migration and trapping patterns seen in much more detailed three-dimensional simulations, while running up to 100 times faster. Although it does not yet include some finer-scale processes such as mixing and dissolution, it captures the dominant flow behavior well. This makes it useful for rapid screening, uncertainty analysis, and planning of carbon storage projects in depleted gas reservoirs.

1 Introduction

Carbon capture, utilization, and storage (CCUS) is a key mitigation strategy for reducing greenhouse gas emissions and supporting global carbon neutrality efforts, particularly for industries that are challenging to decarbonize, including steel, cement, and chemical manufacturing, as well as potential large-scale production of bio-hydrogen [Méndez et al., 2023, Chen et al., 2022, Rosa and Mazzotti, 2022, Wei et al., 2023]. CCUS entails capturing carbon dioxide (CO_2) from industrial emissions or directly from the atmosphere, followed by its transportation for either reuse or permanent underground storage[Krevor et al., 2023, Wareing et al., 2014, Chen et al., 2022, Lau et al., 2021]. One of the most promising methods for permanent CO_2 storage involves injecting it into geological formations such as deep saline aquifers or depleted oil and gas reservoirs [Hepple and Benson, 2004, Kumar et al., 2005, Ringrose et al., 2021, Hamza et al., 2021]. Utilizing depleted oil and gas fields generally offers secure long-term storage, as these formations have retained hydrocarbons beneath impermeable caprocks for millions of years. In some cases, it may also facilitate enhanced hydrocarbon recovery, which can help offset some of the costs related to CO_2 sequestration. Compared to saline aquifers, which can experience pressure build-up and integrity challenges during CO_2 injection, hydrocarbon reservoirs provide a well-documented storage environment with lower pressures and extensive geological data availability. Another significant advantage of depleted reservoirs is the presence of existing infrastructure for CO_2 transport and injection [Hamza et al., 2021, Jenkins et al., 2012, Muhammed et al., 2023, Patel et al., 2016].

A key difference between depleted reservoirs and saline aquifers is the presence of natural gas in depleted gas reservoirs. This adds complexity to the process as contact between CO_2 and the gas causes fluid mixing, leading to the creation of a mixing zone that alters key fluid properties, including density and viscosity, which in turn modifies displacement mechanisms and can induce convective currents that further influence the migration and redistribution of CO_2 and reservoir gas. Therefore, an accurate representation and study of their behavior and interactions are required [Ma et al., 2019, Ghanbari et al., 2020, Liu et al., 2022]. Reservoir simulation serves as a crucial tool for analyzing and studying CO_2 geological storage. Both commercial and open-source simulators are available to represent various scenarios [Class et al., 2009]. To be able to properly define and differentiate CO_2 and natural gas and capture the mixing phenomena, we need to define a multi-component gas phase. Compositional simulations

use Equations of State (EoS) to model multi-component behavior in one or more phases. In this context, CO_2 can be accurately differentiated from hydrocarbons, allowing for accurate modeling of their interactions in the reservoir [Oldenburg and Org, 2003, Al-Hashami et al., 2005, Ghanbari et al., 2020, Liu et al., 2022]. Compositional simulations are computationally intensive because they must perform flash calculations in every gridblock, which typically require more iterations for convergence than models that rely on simplified phase behavior representations. Previous research has explored the application of black oil models to simulate thermodynamic phase behavior in compositional simulations in order to speed up the simulations and maintain accuracy as much as possible. This approach sacrifices some accuracy in favor of cost efficiency, making it particularly useful for uncertainty analysis [Hassanzadeh et al., 2008, Amooie and Moortgat, 2018]. Nonetheless, CO_2 storage simulations still remain computationally intensive due to the large spatial scales and extended timeframes spanning several centuries.

In many cases, the horizontal extent of the reservoir is much larger than the vertical. When there is a significant density difference between fluids and sufficient vertical permeability, gravity causes them to segregate, with heavier fluids settling at the bottom and lighter ones rising to the top. This leads to a state of vertical equilibrium (VE), where fluid saturations vary predictably with depth. The vertical equilibrium assumption allows us to integrate the governing equations over the vertical axis and express them in terms of vertically averaged parameters. As a result, we can simplify a 3D model into a 2D one, which greatly reduces computational cost. This approach, referred to as VE modeling, is increasingly used for simulating large-scale CO_2 plume migration in the subsurface [Nordbotten and Celia, 2011, Bandilla et al., 2019]. Traditionally, VE models applied to CO_2 storage problems have focused on two-phase systems, where the reservoir is initially saturated with brine and CO_2 is injected as a single immiscible gas phase. The most common simplification in early VE models involved complete segregation of fluids with a distinctive interface [Gasda et al., 2009, Nilsen et al., 2016b, Court et al., 2012]. These models have since been extended to include effects such as hysteresis [Doster et al., 2012, 2013, Gasda et al., 2013b], heterogeneity [Guo et al., 2016, Moyner and Nilsen, 2019], dissolution [Gasda et al., 2011, Mykkeltvedt and Nordbotten, 2012], capillary fringe [Nilsen et al., 2016a, Nordbotten and Dahle, 2011], sub-scale topographic variations (rugosity) [Gasda et al., 2012, 2013a, Ahmadinia et al., 2019], fault leakage [Ramachandran et al., 2024], geomechanics [Bjørnarå et al., 2016, Andersen et al., 2017], compressibility [Andersen et al., 2015], and fractured (dual-continuum) reservoirs [March Castaneda Neto, 2018, Guo et al., 2017, Tao et al., 2019]. Additionally, several studies have aimed to relax the assumption of vertical equilibrium for wider applications, including near-wellbore flow, well leakage, and large-scale plume migration in heterogeneous formations [Guo et al., 2014, 2016, Becker et al., 2017, Zheng et al., 2021]. To address the limitations of VE models, particularly near injection wells and heterogeneous reservoir regions, other researchers have explored hybrid approaches that couple between VE and 3D models [Moyner and Nilsen, 2019, Becker et al., 2022, Buntic et al., 2025].

The computational efficiency of VE models makes them particularly valuable for screening studies and statistical analysis workflows that require the simulation of large ensembles. In carbon storage assessment, uncertainty quantification demands evaluation across numerous geological realizations, injection scenarios, and operational parameters—tasks that become computationally impractical with full-physics compositional models. de Jonge Anderson et al. [2024] used reduced-complexity VE models to perform well location and storage capacity assessments in heterogeneous saline aquifers, running thousands of simulations within practical timeframes. Similarly, VE frameworks facilitate the rapid screening of multiple storage sites, robust sensitivity and uncertainty analysis of key parameters affecting plume migration, and probabilistic risk assessment of leakage scenarios [Allen et al., 2018, Tadjer et al., 2021, Pettersson et al., 2022, Anyosa et al., 2024]. For depleted gas reservoirs, where additional uncertainties arise from gas saturation distributions, pressure depletion levels, and CO_2-methane displacement dynamics, the ability to perform comprehensive statistical analysis becomes even more critical.

Building upon the foundational VE modeling work for two-phase systems, two important early contributions extended VE concepts to three-phase flow. The first, by Virnovsky et al. [1996], developed a vertically integrated model for gas-oil-water displacement fronts during water-alternating-gas (WAG) operations. Assuming vertical equilibrium and incompressible, immiscible fluids, the authors derived pseudo relative permeability and capillary pressure functions to reduce 2D gravity-segregated flow into a 1D formulation. This allowed for analytical exploration of front stability through traveling-wave solutions and was among the earliest works to address three-phase VE dynamics and their implications for vertical sweep efficiency. The second, by Guerrero et al. [2013] and Donat et al. [2014], proposed a one-dimensional three-phase VE model incorporating both buoyancy-driven hyperbolic terms and capillarity-driven parabolic terms. They solved the governing equations using high-resolution Weighted Essentially Non-Oscillatory (WENO) schemes coupled with Implicit–Explicit (IMEX) time-stepping strategies. Their work highlighted the numerical challenges of simulating saturation fronts under VE and provided a robust computational approach. Both studies assumed incompressible fluids and made significant strides in capturing multi-phase dynamics within VE frameworks.

In this study, we build upon existing two-phase vertically integrated models by extending them to a three-phase framework. In this approach, CO_2 and methane are treated as two distinct compressible phases, while water is represented as the third, incompressible phase. Our formulation simplifies the problem in two stages: first by reducing a compositional model to a black-oil approximation, and then by collapsing the full 3D representation into a 2D vertically integrated model. This dual simplification enables simulations that are orders of magnitude faster while maintaining reasonable accuracy.

2 Three Phase Vertical Equilibrium Modeling

2.1 Overview and Assumptions

This study examines CO_2 injection into a depleted gas reservoir system that is vertically confined at both upper and lower boundaries. The reservoir structure consists of one or more gas caps with the remaining volume occupied by brine. Due to depletion, the reservoir pressure is anticipated to be below its initial state. The density of CO_2 is substantially lower than brine but higher than methane across all relevant pressure and temperature conditions. CO_2 exhibits non-ideal behavior, with density and viscosity demonstrating significant variations with pressure and temperature changes. The higher viscosity of CO_2 compared to methane effectively suppresses viscous fingering phenomena and promotes the formation of a stable displacement front. The interaction between CO_2 and methane creates a mixing zone at the front whose characteristics are determined by the competing effects of diffusion and dispersion. At elevated pressures, the density contrast between CO_2 and methane increases (see Figure 8), leading to a narrower mixing zone, particularly under stable stratification conditions. Stable stratification develops when the denser CO_2 layer is positioned beneath the lighter methane layer, preventing convective mixing processes. In contrast, when the denser CO_2 layer overlies lighter methane, gravitational instability develops, substantially accelerating mixing dynamics through convective mixing. In configurations where methane is initially positioned above CO_2, mixing is governed by diffusion. The higher viscosity of CO_2 relative to methane creates a mobility ratio that prevents the development of viscous fingering instabilities [Oldenburg et al., 2001]. Numerical simulations indicate that after CO_2 injection stops, the stored CO_2 continues to sink beneath the overlying methane under density and pressure gradients, forming stratified layers while the mixing zone gradually expands through molecular diffusion [Oldenburg et al., 2001]. Methane is far less dense and viscous than water, so it separates quickly. By contrast, O_2 is less viscous than water but, at higher reservoir pressures, can have a density approaching that of water. It is still typically slightly buoyant and will disengage from the aqueous phase, though with a smaller density

contrast than methane [Ghanbari et al., 2020].

The conventional black oil modeling framework lacks the capability to define multi-component gas phases. Compositional simulation approaches incorporate equations of state to predict fluid properties and phase interactions under varying pressure and temperature conditions by accounting for the characteristics of individual components. For computational simplicity, this study assumes that the gas plume within the reservoir consists exclusively of methane. The initial compositional model to simulate CO_2 injection into the depleted gas reservoir is developed using the MATLAB Reservoir Simulation Toolbox (MRST) compositional module and subsequently transferred to Jutul Darcy, a high-performance simulator that offers significantly faster computational performance [Lie, 2019, Moyner, 2024]. The model initialization incorporates two-phase saturations comprising an aqueous phase (water) and a gaseous phase (methane), with methane occupying the upper reservoir zones and hydrostatic pressure distribution specified throughout the domain. The system is characterized as a three-phase model encompassing water, oil, and gas phases, where the oil and gas phases represent liquid and vapor phases calculated through equation of state modeling. However, given that both methane and CO_2 possess extremely low critical temperatures of -82.59°C and 31.8°C respectively, both components are represented as gas phase constituents in typical reservoir conditions. Consequently, no oil (liquid) phase exists during the simulations, effectively reducing the system to a two-phase water-gas system. To isolate the fundamental CO_2-methane-water displacement mechanisms, water is treated as incompressible with no dissolution effects, and capillary pressure is neglected. These simplifications enable focus on capturing the essential reservoir processes while serving as an initial framework for subsequent detailed modeling efforts. Molecular diffusion and dispersion processes are excluded from this analysis. Although these physical mixing mechanisms are not explicitly incorporated in the model, a mixing zone between fluids can still develop during simulation due to numerical dispersion, which is inherent to the discretization methods employed for solving the governing flow equations. The magnitude of this numerical dispersion depends on factors such as grid resolution, meaning that the observed mixing in simulation results reflects the chosen numerical scheme and may not directly correspond to actual physical mixing processes [Haajizadeh et al., 1999, Shrivastava, 2003, Ghanbari et al., 2018, 2020].

The VE model aims to simulate three-dimensional aquifer systems with substantial horizontal extent using two-dimensional representations through the solution of integrated 2D governing equations. This upscaled model formulation relies on the fundamental assumption of VE, requiring the absence of flow perpendicular to the aquifer plane. This assumption must remain valid across the relevant spatial and temporal scales of the system. While VE models can accommodate various physical effects including hysteresis, solubility, and capillary phenomena, the primary objective of this study is to develop a formulation that incorporates CO_2 and methane in a manner consistent with 3D compositional simulations and to evaluate the resulting model performance. Several simplifications are therefore adopted: rock and brine phases are treated as incompressible, no flow occurs through top and bottom boundaries, dissolution and capillary fringe effects are neglected, residual saturations are assumed to be zero, and isothermal conditions are maintained throughout the reservoir. Additionally, mixing phenomena are excluded from the vertical equilibrium model. While this approach ignores the miscible behavior of CO_2 and methane, it preserves the computational benefits of VE modeling while extending its capability to capture key multiphase flow phenomena. We are hence reprenting the water-gas phase system with water, CO_2 and methane components as a three phase system where each phase represents a component. We show with the help of representative scenarios that due to strong gravity segregation of CO_2 and methane this mixing is a second order effect while first order displacement dynamics, such as the CO_2 plume extent and gas–water contact shape, are captured well with our approach.

The ad-core module within MRST provides an object-oriented framework for rapid prototyping of reservoir simulators based on automatic differentiation. This framework facilitates the

modification and extension of existing simulation models in MRST or the implementation of new ones. This framework is used to apply the three-phase VE formulation discussed in the following section. The development focuses on an h-formulation system of equations where the primary variables are plume heights rather than saturations, offering a more intuitive representation for VE models.

2.2 Governing Equations

This section presents the governing equations for a three-phase vertical equilibrium (VE) model designed for multiphase flow in porous media, with particular application to CO_2 storage in depleted gas reservoirs. The model considers a vertically stratified system containing methane, CO_2, and water, arranged according to their densities under the assumption of rapid vertical pressure equilibration. The emphasis is placed on the fundamental assumptions and simplifications inherent in the VE framework, rather than addressing the complexity of reservoir heterogeneity or boundary conditions. Throughout this work, lower-case symbols denote fine-scale, three-dimensional quantities, while the corresponding upper-case symbols (introduced later) represent vertically integrated, VE-scale quantities.

The system under consideration involves three immiscible phases flowing through a rigid porous medium under isothermal conditions. The fluid phases are denoted as brine (b), carbon dioxide (c), and methane (m), ordered by density such that $\rho_b > \rho_c > \rho_m$. Each phase occupies a portion of the pore space, and their respective saturations satisfy the constraint.

$$s_b + s_c + s_m = 1 \tag{1}$$

The mass conservation principle for each fluid phase $\alpha \in b, c, m$, representing brine, CO_2, and methane respectively, is expressed through the three-dimensional mass balance equation:

$$\frac{\partial}{\partial t}\left(\rho_\alpha \phi s_\alpha\right) + \nabla \cdot \rho_\alpha \mathbf{u}_\alpha = \psi_\alpha \tag{2}$$

In this formulation, ϕ represents the porosity, s_α denotes the saturation of phase α, $\mathbf{u}_\alpha$ is the corresponding Darcy velocity, and ψ_α accounts for sources or sinks. The velocity field $\mathbf{u}_\alpha$ follows Darcy's law:

$$\mathbf{u}_\alpha = -\frac{k k_{r\alpha}}{\mu_\alpha}\left(\nabla p_\alpha - \rho_\alpha \mathbf{g}\right) \tag{3}$$

Here, k denotes the absolute permeability, $k_{r\alpha}$ is the relative permeability to phase α, μ_α is the viscosity of phase α, p_α is the pressure of phase α, and $\mathbf{g}$ is the gravitational acceleration vector. In order to derive a vertically integrated flow model, we integrate the mass balance equation (2) over the vertical coordinate, z, from the bottom boundary ζ_B to the top boundary ζ_T:

$$\int_{\zeta_B}^{\zeta_T} \left[\frac{\partial}{\partial t}(\rho_\alpha \phi s_\alpha) + \nabla \cdot (\rho_\alpha \mathbf{u}_\alpha)\right] dz = \int_{\zeta_B}^{\zeta_T} \psi_\alpha \, dz \tag{4}$$

The objective is to express the resulting upscaled equation based on variables that depend solely on the horizontal spatial coordinates (x, y) and time t. Assuming there is no vertical flow through the top and bottom boundaries (i.e., $\mathbf{u}_{\alpha,z} = 0$ at $z = \zeta_B$ and $z = \zeta_T$), and that the boundaries are stationary, the Leibniz rule for differentiation under the integral sign can be applied. This procedure yields the vertically integrated equation:

$$\frac{\partial}{\partial t}\left(\int_{\zeta_B}^{\zeta_T} \rho_\alpha \phi s_\alpha \, dz\right) + \nabla_\parallel \cdot \left(\int_{\zeta_B}^{\zeta_T} \rho_\alpha \mathbf{u}_{\alpha,\parallel} \, dz\right) = \int_{\zeta_B}^{\zeta_T} \psi_\alpha \, dz \tag{5}$$

where $\nabla_\parallel$ and $\mathbf{u}_{\alpha,\parallel}$ refer to the horizontal components of the gradient and velocity, respectively. To proceed with the formulation, it is necessary to introduce several quantities that have been

integrated over the vertical coordinate. These vertically integrated variables are defined as follows:

$$\Phi := \int_{\zeta_B}^{\zeta_T} \phi \, dz \tag{6}$$

$$S_\alpha := \frac{1}{\Phi} \int_{\zeta_B}^{\zeta_T} \phi s_\alpha \, dz \tag{7}$$

$$R_\alpha := \frac{1}{\Phi S_\alpha} \int_{\zeta_B}^{\zeta_T} \rho_\alpha \phi s_\alpha \, dz \tag{8}$$

$$\Psi_\alpha := \int_{\zeta_B}^{\zeta_T} \psi_\alpha \, dz \tag{9}$$

$$\mathbf{U}_\alpha := \int_{\zeta_B}^{\zeta_T} \mathbf{u}_{\alpha,\parallel} \, dz \tag{10}$$

$$\mathbf{F}_\alpha := \int_{\zeta_B}^{\zeta_T} \rho_\alpha \mathbf{u}_{\alpha,\parallel} \, dz \tag{11}$$

Here, Φ denotes the vertically integrated porosity, S_α is the upscaled saturation, and R_α refers to the upscaled density of phase α. The term $\mathbf{U}_\alpha$ corresponds to the total horizontal volumetric flux, while $\mathbf{F}_\alpha$ indicates the total horizontal mass flux of phase α across the vertical column. The term Ψ_α represents the integrated source or sink for phase α over the vertical domain. Substituting these expressions into equation (5) yields the vertically integrated mass balance equation:

$$\frac{\partial}{\partial t} \left(R_\alpha \Phi S_\alpha \right) + \nabla_\parallel \cdot \mathbf{F}_\alpha = \Psi_\alpha \tag{12}$$

This vertically integrated formulation accounts for variable density effects, enabling accurate modeling of density variations throughout the system [Andersen et al., 2015]. To evaluate the integral of the phase's lateral mass flux, we incorporate equation (3) into equation (11), yielding:

$$\mathbf{F}_\alpha = - \int_{\zeta_B}^{\zeta_T} \rho_\alpha \lambda_\alpha k_\parallel \nabla_\parallel \, p_\alpha \, dz \tag{13}$$

The evaluation of this integral requires the reconstruction of fine-scale quantities based on coarse scale (upscaled) variables, which can vary depending on the specific modeling approach and physical context. Certain variables like porosity ϕ and permeability k are predetermined inputs while others are reconstructed from upscaled quantities under specific assumptions. For the pressure gradient $\nabla_\parallel p_\alpha$ and the density ρ_α, these quantities are expressed relative to reference values, with the fundamental reference quantity being the reference pressure, termed upscaled pressure P_α in this formulation. This upscaled pressure represents a two-dimensional field that varies spatially across the horizontal domain (x_1, x_2) and serves as the primary pressure variable in the VE formulation. Under the VE assumption, the pressure of each phase p_α varies hydrostatically in the vertical direction according to:

$$\frac{\partial p_\alpha}{\partial z} = -\rho_\alpha g \tag{14}$$

The total hydrostatic pressure change between two vertical depths a and b is determined by integrating this expression:

$$\Delta p_\alpha = - \int_a^b \rho_\alpha g \, dz \tag{15}$$

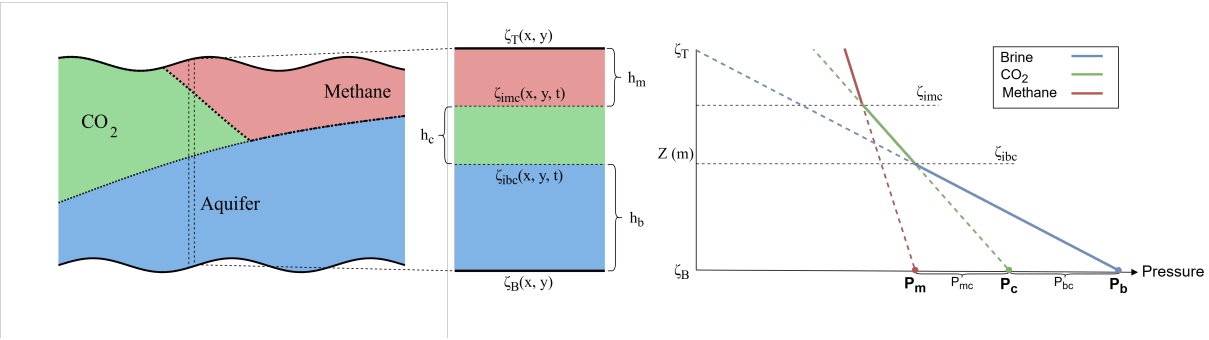

Figure 1: A schematic of phase interfaces and plume heights

This relationship allows the vertical pressure profile to be reconstructed from an upscaled phase pressure, typically taken at either the bottom or top of the column. Denoting the phase-specific pressure at the bottom as $P_\alpha(x_1, x_2, t)$, the vertical pressure distribution for each phase under equilibrium conditions is written as:

$$p_\alpha(x_1, x_2, z, t) = P_\alpha(x_1, x_2, t) - g \int_{\zeta_B}^{z} \rho_\alpha dz' \tag{16}$$

To proceed with the formulation, we must define the phase densities. In our case, brine is assumed to be incompressible, while the densities of CO_2 and methane vary with pressure under the assumption of constant temperature. We capture this relationship by fitting an equation to equation-of-state (EoS) data, as described in A. A key challenge arises because we are only solving for the VE reference (bottom) pressure rather than for the entire column, and we need to provide the density values across the interval. Consequently, we must incorporate a density profile that depends on the hydrostatic pressure distribution—which itself depends on the density at other points. This interdependence introduces a nonlocal effect. The most direct approach would involve numerically reconstructing the full vertical density profile at every timestep and integrating across the column, but this method is computationally expensive.

To avoid this computational cost, a Taylor series expansion is employed that allows representation of a function locally in terms of its value and derivatives at a reference point. In this context, the expansion is applied to the density functions of the compressible phases to approximate their density profile over their respective phase fluid columns. By integrating this approximated density function over each fluid column, an "upscaled" density equation is obtained that corresponds to the total mass of that phase in the column. We limit the Taylor series to second-order terms and expand around a reference pressure (i.e., the upscaled pressure), which leads to the following density equation:

$$\rho_\alpha(p) \approx \rho_\alpha(p_{ref}) - \frac{\rho'_\alpha(p_{ref})}{1!}\rho_\alpha(p_{ref})g[z - \zeta_{ref}] + \frac{\rho''_\alpha(p_{ref})}{2!}(\rho_\alpha(p_{ref})g[z - \zeta_{ref}])^2 \tag{17}$$

This expression is valid for any reference point situated within the reservoir's height. In this study, we chose the bottom of the reservoir as the reference point, meaning the phase pressures at this depth are taken as the reference pressure. A similar Taylor series approach is adopted for representing viscosity. For flux calculations, the formulation is simplified by retaining only the zeroth-order terms of both density and viscosity, ignoring higher-order terms and evaluating them at a single reference pressure:

$$\rho_\alpha(p) \approx \rho_\alpha(p_{ref}), \quad \mu_\alpha(p) \approx \mu_\alpha(p_{ref}) \tag{18}$$

This approximation implies that density and viscosity variations along the vertical coordinate are negligible, enabling these terms to be factored out of vertical integrals.

To efficiently address the system of equations, standard practice involves selecting and solving explicitly for a single-phase pressure, with the pressures of other phases expressed relative to this reference through pressure differences. The vertical domain is divided into distinct regions by phase interfaces located at $\zeta_{i\alpha\beta}$, where adjacent phases α and β meet. At these interfaces, the pressure difference between two adjacent phases is defined by subtracting the hydrostatic contribution from each other:

$$p_{\alpha\beta} = P_{\alpha\beta} - g \int_{\zeta_B}^{\zeta_{i\alpha\beta}} (\rho_\alpha - \rho_\beta)\, dz \tag{19}$$

When fine-scale effects like capillary pressure are neglected, the pressure difference between each pair of phases at the interfaces becomes zero. This simplification reduces the equations to:

$$P_{\alpha\beta} = g \int_{\zeta_B}^{\zeta_{i\alpha\beta}} (\rho_\alpha - \rho_\beta)\, dz \tag{20}$$

Incorporating the density approximation eq (18) into the upscaled pressure difference equations yields:

$$P_{\alpha\beta} = (\rho_\alpha(P_\alpha) - \rho_\beta(P_\beta))\, g\, (\zeta_{i\alpha\beta} - \zeta_B) \tag{21}$$

Here, P_β refers to the phase β pressure at the bottom, and the subscripts α and β represent any two adjacent phases in the multi-phase system. However, this choice introduces a circular dependency: the upscaled pressure difference needed to calculate the phase β pressure from the phase α pressure depends on the phase β density, while the phase β density itself requires knowledge of the phase β pressure. Solving this implicit coupling directly would demand iterative reconstruction of the phase β pressure at every timestep, which is computationally expensive. To avoid this computational complexity, we expand $\rho_\beta(P_\beta)$:

$$\begin{aligned} \rho_\beta(P_\beta) &= \rho_\beta(P_\alpha + P_{\alpha\beta}) \\ &\approx \rho_\beta(P_\alpha) + \left.\frac{\partial \rho_\beta}{\partial P}\right|_{P_\alpha} \cdot P_{\alpha\beta} \end{aligned} \tag{22}$$

In our formulation, CO_2 pressure is the primary unknown variable we solve for (phase α), with water and methane as phase β. Since water is incompressible and methane is weakly compressible, the density derivative $\left.\frac{\partial \rho_\beta}{\partial P}\right|_{P_\alpha}$ becomes zero or negligible. Additionally, pressure differences are small relative to absolute pressures in the system. These conditions allow us to evaluate phase β density at the phase α pressure (P_α) rather than the phase β pressure (P_β), which eliminates the circular dependency and simplifies the pressure difference equations to depend only on phase α pressure. Additionally, the interface depths are subsequently expressed in terms of phase thicknesses as follows:

$$\begin{aligned} brine: &\quad h_b \equiv \zeta_{ibc} - \zeta_B \\ carbon\,dioxide: &\quad h_c \equiv \zeta_{imc} - \zeta_{ibc} \equiv H - h_m - h_b \\ methane: &\quad h_m \equiv \zeta_T - \zeta_{imc} \end{aligned} \tag{23}$$

Where $H = \zeta_T - \zeta_B$. Here, the CO_2 phase height is expressed as a function of the brine and methane heights, thereby reducing the number of independent unknowns, in a manner similar to three-phase black-oil models where saturations are the primary variables. These changes yield phase-specific equations for CO_2-brine and CO_2-methane as follows:

$$P_{bc} = (\rho_b - \rho_c(P_c))\, g\, h_b \tag{24}$$

$$P_{mc} = (\rho_c(P_c) - \rho_m(P_c))\, g\, (H - h_g) \tag{25}$$

Based on the new density and phase height expressions, we reformulate the pressure equations and compute the lateral pressure gradients for each phase. Assuming an incompressible brine and CO_2 and methane densities independent of the vertical coordinate, along with negligible lateral variations in density and gravitational effects, we obtain the following phase-specific expressions for $\nabla_{\|}\, p_\alpha$:

$$\nabla_{\|} p_\alpha = \nabla P_\alpha + \rho_\alpha(P_\alpha) g \nabla \zeta_B \tag{26}$$

Note that the final pressure gradients are not a function of z and are taken out of the integral in equation (13). We now define other vertically integrated variables as follows:

$$K := \int_{\zeta_B}^{\zeta_T} k_{\|}\, dz \tag{27}$$

$$\Lambda_\alpha := \frac{1}{K} \int_{\zeta_B}^{\zeta_T} \lambda_\alpha\, k_{\|}\, dz \tag{28}$$

$$\tilde{R}_\alpha := \frac{1}{K\, \Lambda_\alpha} \int_{\zeta_B}^{\zeta_T} \rho_\alpha \lambda_\alpha\, k_{\|}\, dz \tag{29}$$

Where K and Λ_α are vertically integrated permeability and mobility terms, respectively. The variable $\tilde{R}_\alpha$ is introduced to account for density effects in the integrated flux term. Specifically, $\tilde{R}_\alpha$ is defined as the upscaled phase density weighted by mobility and permeability. When assuming either incompressible fluids or compressible fluids with no dependence on the vertical coordinate (i.e., equation (18)), the density is taken outside the integral, resulting in:

$$\tilde{R}_\alpha = \begin{cases} \rho_\alpha, & \alpha = b, \\ \rho_\alpha(P_{ref}), & \alpha \in \{c, m\}. \end{cases} \tag{30}$$

Having established the vertically integrated density $\tilde{R}_\alpha$, we now turn to the pressure gradient term in Darcy's equation (3). In the special case of a fully homogeneous reservoir ($k_{\|} = k = \text{const}$), a sharp-interface model with no residual saturations (λ_α takes only saturation values of 0 or 1), the constant permeability moves out of the integrals. This permits analytical integration and allows Λ_α to be explicitly defined for each phase:

$$\Lambda_\alpha \; = \frac{k}{kH} \int_{\zeta_B}^{\zeta_T} \lambda_\alpha\, dz \; = \lambda_\alpha(1) \frac{h_\alpha}{H}. \tag{31}$$

The flow interaction between CO_2 and methane is modeled using a shared relative permeability curve for both components, consistent with the conventional compositional approach in which they are treated as a single phase. Consequently, the endpoint mobilities for the two components share the same relative permeability value at full saturation, meaning $k_{rm}(1) = k_{rc}(1)$. As given in equation (18), the viscosity terms in λ_α do not vary with the vertical coordinate and can therefore be pulled out of the integral.

The final upscaled mass flux terms for each phase are written using the coarse-scale permeability and mobilities as:

$$\mathbf{F}_\alpha = -\tilde{R}_\alpha \Lambda_\alpha K (\nabla P_\alpha + \rho_\alpha(P_\alpha)\, g \nabla \zeta_B). \tag{32}$$

Returning to the upscaled mass accumulation term in equation (8), for a homogeneous reservoir and given that saturation is either zero or one, we can restrict the integration domain for each phase to the vertical interval where its saturation is one. This simplifies equation (8) to:

$$R_\alpha \Phi S_\alpha = \phi \int_{\zeta_a}^{\zeta_b} \rho_\alpha \, dz, \quad \{a, b\} \in \{B, ibc, imc, T\} \tag{33}$$

Where ζ_a to ζ_b denotes the vertical region occupied entirely by the phase α. For brine, which is incompressible, density can be taken outside the integral, yielding a simplified expression. For CO_2 and methane density functions, however, rather than neglecting higher-order terms, we retain them and evaluate the vertical integral of the density function from equation (17), resulting in:

$$R_\alpha = \rho_\alpha(p_a)[\zeta_b - \zeta_a] - \frac{\rho'_\alpha(p_a)}{1!}(\rho_\alpha(p_a)g)\frac{[\zeta_b - \zeta_a]^2}{2} + \frac{\rho''_\alpha(p_a)}{2!}(\rho_\alpha(p_a)g)^2\frac{[\zeta_b - \zeta_a]^3}{3}, \quad \{\alpha\} \in \{c, m\} \tag{34}$$

This expression is then used in the mass accumulation term for CO_2 and methane, where the reference pressure matches that used in the upscaled phase density of the flux term. The final vertically integrated flow equations become the following:

$$-\Phi\frac{\partial(R_\alpha S_\alpha)}{\partial t} + \nabla \cdot \mathbf{F}_\alpha = \Psi_\alpha \tag{35}$$

The vertically integrated equations derived above were implemented in the MATLAB Reservoir Simulation Toolbox (MRST) using its Automatic Differentiation framework [Lie and Møyner, 2021]. The approach uses plume heights as the primary variables and calculates phase fluxes based on vertically averaged mobilities and hydrostatic pressure gradients, consistent with VE assumptions. This setup retains the analytical structure of the VE formulation while utilizing MRST's ADI capabilities for residual construction, Jacobian computation, and fully implicit time integration, ensuring both robustness and scalability.

3 Results and Discussion

This section shows the results from three case studies using the three-phase VE model developed in this work, and compares them to compositional simulations. The first case uses a flat, layered synthetic reservoir to benchmark the VE model against compositional simulations in an idealised geometry. The second looks at a dual-anticline structure to assess grid sensitivity and structural trapping behavior. The third applies the model to the real-world Hugin Formation East to evaluate its performance in a geologically realistic field setting. As described earlier, the initial compositional models were built with the MRST compositional module, then transferred and executed in Jutul Darcy. Simulations were carried out either on a local workstation with an Intel Core i9-14900K processor or on the DMOG HPC cluster. Some simulations also used MPI-based parallel computing to speed up the runtimes. Brine properties are treated as incompressible in both the compositional and VE models, using constant values of 1000 kg m^{-3} for density and 1 cP for viscosity. In the VE model, methane and CO_2 are treated as compressible fluids, with their density and viscosity defined by pressure-dependent correlations, as outlined in Section 2. The compositional model uses an equation of state (EoS) to compute the thermophysical properties of methane and CO_2.

3.1 Case 1 — Flat-Layered Gas–Brine Benchmark

The first case study features a simplified flat-layered synthetic reservoir model, designed as a benchmark scenario to study basic flow behavior in compositional simulations. The model has a uniform structure with no topographic variation and spans 10 kilometers in the horizontal direction with a constant vertical thickness of 50 meters. The domain is initialized with the upper half of the reservoir saturated with methane, while the lower half contains brine, representing a

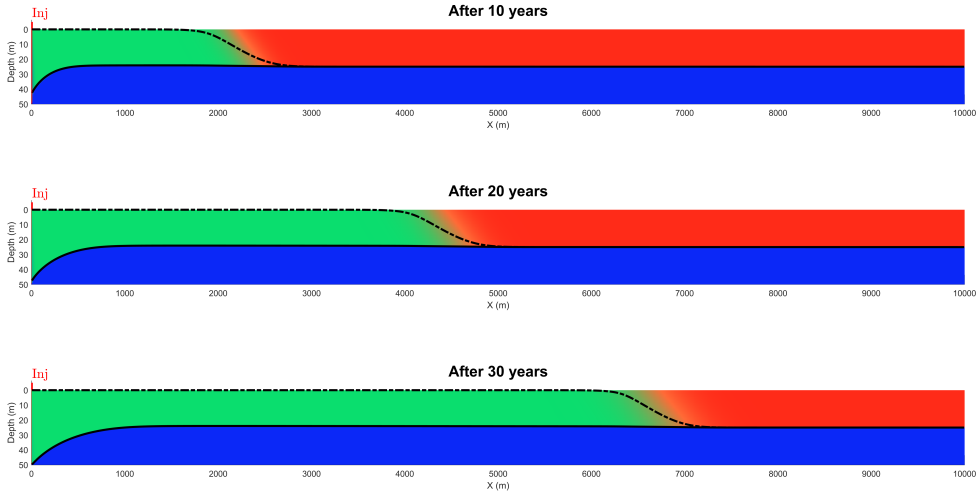

Figure 2: Compositional simulation (colored fields) versus VE model predictions (black lines) for Case 1. The VE model approximates the CO_2 (green) plume's migration into methane (red) and along the brine (blue) interface at 10, 20, and 30 years.

stratified two-phase system. The reservoir pressure is set to 150 bar at the gas–water interface, with a hydrostatic pressure distribution applied throughout the domain. The porosity is set uniformly at 20%, and the permeability is isotropic, with values of 100 mD. The reservoir is discretized into a structured grid with 1000 horizontal cells ($dx = 10\,\mathrm{m}$) and 100 vertical layers ($dz = 0.5\,\mathrm{m}$), yielding a total of 100,000 grid cells. Injection is performed from a well at the left side at a constant rate of 2000 kg/day for a period of 30 years, while the right boundary maintains constant hydrostatic pressure.

Figure 2 compares the fine-grid compositional simulation to the three-phase VE model for the benchmark scenario. The compositional model shows a more diffuse and vertically mixed transition zone between CO_2 and methane, particularly farther from the injection well, whereas the VE model effectively approximates the leading front of the CO_2 plume as it displaces the methane gas at the top of the reservoir. Agreement is especially strong at the brine–CO_2 interface, where the VE model closely follows the lower boundary of the migrating plume. These results confirm that, despite its simplified assumptions, the VE model captures the key large-scale displacement and plume geometry. Its sharp interface approximation provides a robust match to the dominant flow behavior observed in the compositional simulation.

A key observation in this scenario is that, despite CO_2 being co-injected into both brine- and methane-saturated zones, the majority of the CO_2 plume preferentially migrates upward into the methane-rich region, while its advancement within the brine zone is comparatively slower. This response is governed primarily by fluid mobility contrasts in a pressure-driven system, with gravity exerting an influence through gravitational segregation. In particular, CO_2 displacing methane is more favorable than CO_2 displacing water because the CO_2–methane mobility ratio is closer to unity than the CO_2–brine mobility ratio. This setup serves as a reference to validate fluid behavior and mobility under simplified conditions before moving on to more geologically complex cases.

3.2 Case 2 — Dual-Anticline Grid-Sensitivity Benchmark

In the second scenario, a two-dimensional reservoir with a sinuous geometry and two anticlines was used to examine CO_2 plume migration under geologically realistic conditions. The initial

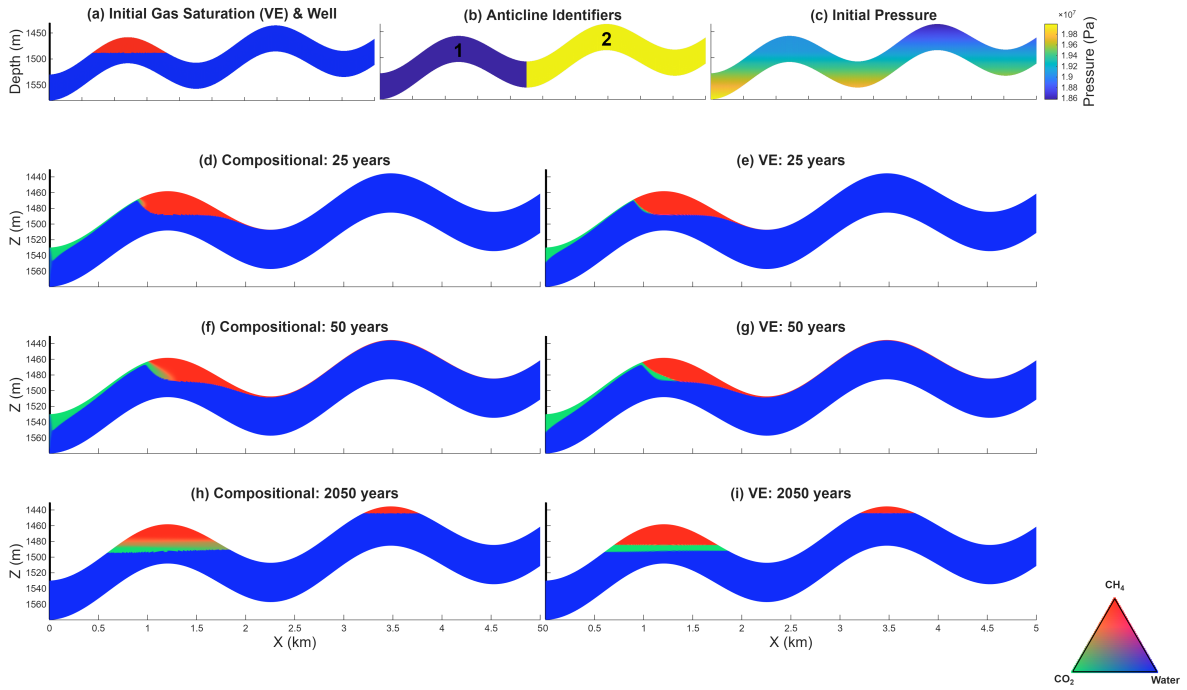

Figure 3: Structural reservoir model and temporal evolution of gas migration. Top row: (a) Initial gas saturation (methane shown in red) and injection well location; (b) Domain segmentation highlighting individual anticline structures used for mass balance tracking; (c) Initial hydrostatic pressure distribution (Pa) across the 5 km domain. Rows 2–4: Comparison of gas plume migration between the Compositional model (left column: d, f, h) and the VE model (right column: e, g, i) at 25, 50, and 2050 years. The snapshots illustrate the displacement of the initial methane (red) by the injected CO_2 (green) and the subsequent structural trapping within the anticline formations.

gas–brine configuration, with a 30-meter-thick gas cap in the left anticline and the remainder of the reservoir saturated with water, is shown in Figure 3a, while the subdivision of the domain into two indexed anticline compartments used for subsequent analysis is shown in Figure 3b. CO_2 is injected at a constant rate of 25 t/year for 50 years through a well located at the left boundary. A constant hydrostatic pressure was maintained at the right boundary, and all other boundaries were treated as no-flow. The simulation continued for 2000 years after injection ceased. The initial pressure at the deepest point in the reservoir was set to 200 bar, and the resulting hydrostatic pressure field is illustrated in Figure 3c, with pressures across the domain calculated based on local fluid saturations. The model domain extends 5 km laterally, 50 m vertically, and 1 m in width, with uniform rock properties defined by a porosity of 20% and a permeability of 10 mD.

Compositional simulations were performed on a refined grid to provide a converged reference solution for comparison with the VE model. The comparison focuses on the predicted redistribution of CO_2 and methane between the two anticlines, as illustrated by the time evolution of phase distributions in the bottom panels of Figure 3, where the compositional results are shown alongside the VE model. To further examine the behaviour in each structure, two indexed regions in the anticlines were tracked over time (see Figure 3b), and the corresponding evolution of CO_2 and methane mass in each compartment is summarized in Figure 4.

The mass balance evolution in each anticline, shown in Figure 3 and Figure 4, is used to compare the VE model against the compositional reference solution. The comparison focuses on

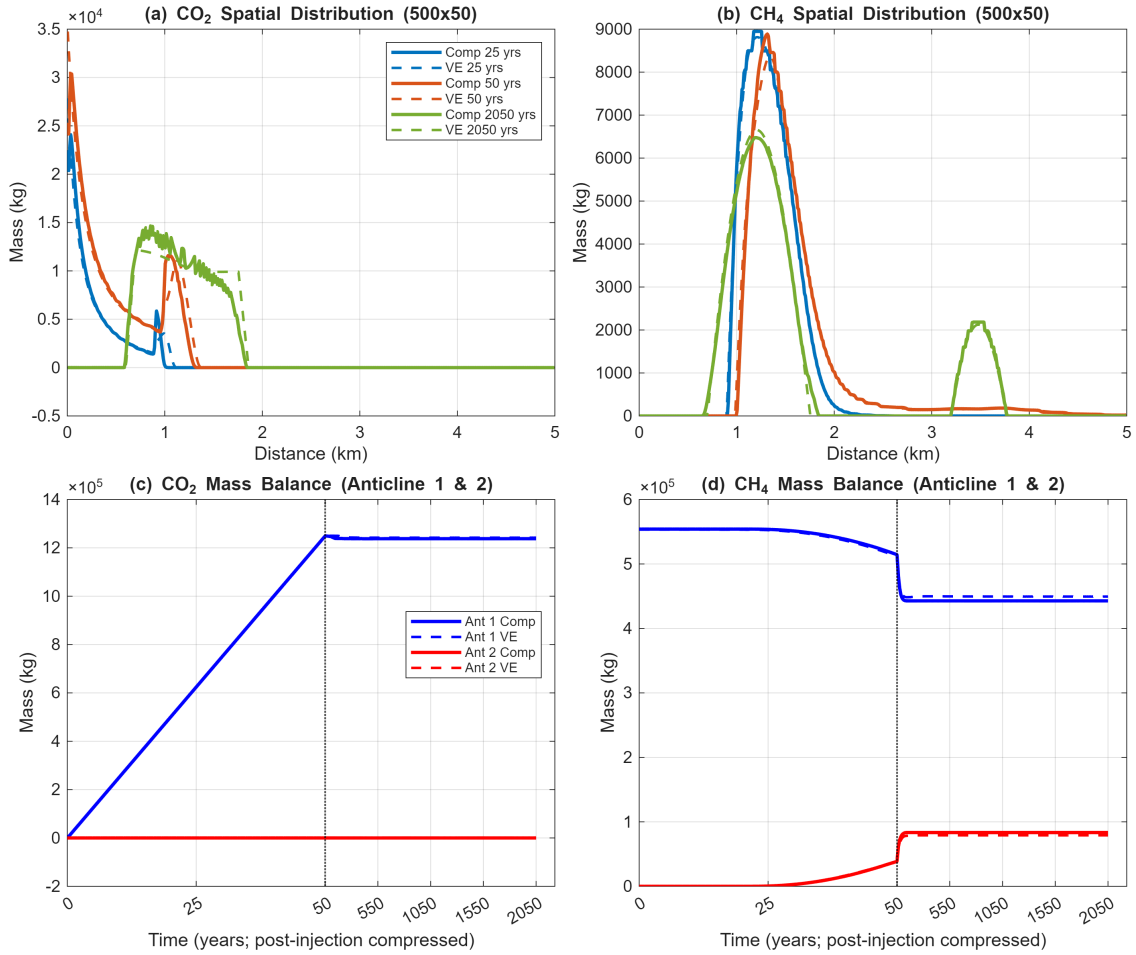

Figure 4: Spatial distribution and mass balance analysis for CO_2 and methane. (a) CO_2 spatial distribution along the domain at 25, 50, and 2050 years. (b) Methane spatial distribution showing the migration and attenuation of the gas plume over time. (c) Cumulative CO_2 mass balance within Anticline 1 and Anticline 2, showing primary containment in Anticline 1. (d) Methane mass balance illustrating the secondary migration from Anticline 1 to Anticline 2. Solid lines indicate the full compositional model (Comp), while dashed lines represent the Vertical Equilibrium (VE) approximation.

the redistribution of CO_2 and methane between the two structural compartments and on the corresponding component inventories over time. Overall, the VE results reproduce the main trends of the compositional model, including the partitioning of mass between the anticlines and its temporal evolution. Since the compositional model is taken here as the reference solution, the purpose of this comparison is to assess how well the VE formulation captures the large scale migration behaviour relevant to this case. It should also be noted that the compositional model does not include molecular diffusion or hydrodynamic dispersion.

3.3 Case 3 — Field-scale demonstration: Hugin Formation East

The third study uses the publicly available *Hugin Formation East* dataset from the CO_2 Storage Atlas of the Norwegian Continental Shelf [Bjørnestad et al., 2017]. The Hugin Formation, located in the South Viking Graben of the North Sea, comprises Middle Jurassic shallow-marine and marginal-marine sandstones deposited during a regional transgression. Here, we use the averaged formation values across the whole formation ($\phi = 12.45$ %, $k = 500$ mD). The simulation grid is a corner-point mesh that honours the complex geometry: 2264×20 cells (horizontal $\times$ vertical)

for a total of 45 280 active cells, covering $\sim 2.26 \times 10^3\,\mathrm{km}^2$ with layer thicknesses ranging from 5.8 to 106.4 m.

The model was initialized with 15 % methane gas and 85 % brine in every cell. A preliminary run is performed so that pressure and saturations relax to hydrostatic equilibrium; this state becomes the initial condition for the main study. A single injector, placed near the structural center, injects $2.5\,\mathrm{Mt\,yr}^{-1}$ of CO_2 for 50 years. After shut-in, the simulation continues for 1 000 years to capture the post-injection redistribution and trapping processes. Figure 6 shows a top view of the compositional simulations compared to the VE model after 10, 50 and 1050 years.

10 years. Both models predict nearly identical plume footprints. The VE solution appears smoother because it integrates over the vertical direction and is therefore insensitive to vertical resolution or the precise shape of the relative-permeability curves.

50 years (end of injection). The plume has migrated downdip beneath the pre-existing methane cap. Crucially, both models place the leading edge at virtually the same x–y location, confirming that the VE model captures the dominant buoyancy- and mobility-controlled dynamics.

1050 years (end of migration). CO_2 primarily occupies the smaller anticlines close to the injection site, displacing the methane that originally resided there into larger and shallower structural traps. The VE model captures the overall redistribution pattern well but underpredicts methane displacement in smaller anticlines, compared to the compositional model. This discrepancy arises in part from numerical dispersion in the compositional model, where coarse grid resolution leads to exaggerated mixing and overestimation of methane movement. However, the VE model also contributes to this difference by excluding mixing processes altogether, which limits its ability to fully represent gas displacement dynamics. The transition zone between CO_2 and methane within the larger gas caps is similarly influenced by both numerical dispersion in the compositional model and the absence of mixing in the VE formulation.

Another key difference lies in the amount of trapped gas predicted by the two models. The VE model uses an analytical approach to estimate vertical saturation, making it independent of vertical grid resolution. In contrast, the 3D compositional model relies on explicit gridding, which can lead to the uppermost cells in smaller anticlines being fully saturated with gas. As a result, the VE model tends to predict a thinner gas column in these regions. This discrepancy, therefore, is due to differences in vertical resolution and the level of detail in the grid discretization.

Overall, the VE model reproduces the dominant features of plume evolution, structural trapping, and long-term redistribution while running orders of magnitude faster than the full compositional calculation, as quantified by the comparison of simulation times in Table 1. This makes VE modelling a powerful tool for rapid field-scale screening and optimisation of prospective CO_2 storage sites, particularly where millennial-scale performance must be evaluated across many geological realizations.

Table 1: Comparison of Simulation Times for Compositional and VE simulations

Scenario	**Compositional (s)**	**VE (s)**
Case 1	15228	36
Case 2	65952	42
Case 3	72360	330

3.4 Discussion

The present study extends the well-established VE modeling framework to account for flow involving CO_2, methane, and brine in depleted gas reservoirs. While previous applications of VE models have demonstrated their utility in simulating the large-scale migration of CO_2 in two-phase (i.e., CO_2-brine) systems with significant computational savings (Gasda et al., 2009;

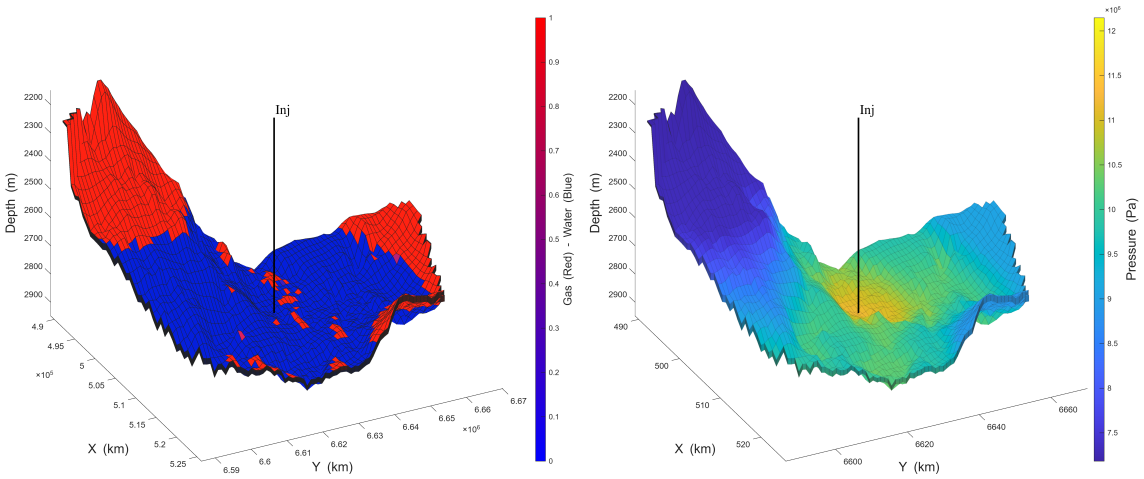

Figure 5: Case 3, Initial saturation and pressure distribution shown from two viewing angles.

Nordbotten and Celia, 2011; Court et al., 2012), their application to depleted gas fields has not previously been explored.

Across all three case studies, the three-phase VE formulation reproduced the large-scale behavior seen in compositional simulations. (i) *Flat, layered benchmark:* the VE model accurately captured the migration of CO_2 into the methane layer and the shape of the CO_2-brine interface. (ii) *Dual anticlines:* the VE model compared well with the compositional simulations, reproducing the large-scale plume geometry and inter-anticline mass redistribution; a supplementary outcome of this test was that the comparison also revealed a strong sensitivity of compositional results to vertical grid resolution. (iii) *Field scale (Hugin Formation):* the VE model successfully replicated the plume migration, structural trapping, and long-term redistribution predicted by the compositional model, confirming its applicability to realistic geological settings.

Across all three cases, certain model limitations became apparent, primarily stemming from the fundamental assumptions of the VE framework. The most significant limitation is the model's current inability to simulate mixing between CO_2 and methane. The current formulation treats CO_2 and methane as immiscible phases with a sharp interface. Consequently, the model cannot replicate phenomena driven by convective mixing, which may be important in scenarios involving direct injection into methane-saturated zones or in highly heterogeneous formations. These limitations are largely due to the core assumptions of the VE method itself, rather than just the fact that it doesn't model mixing. This simplification, while enabling computational speedup, resulted in some discrepancies in predicted volumes of displaced CO_2 and methane within structural traps, particularly when compared to compositional simulations. Additionally, the current formulation excludes other physical mechanisms known to enhance long-term trapping, namely the dissolution of CO_2 into brine and capillary fringe effects, though these mechanisms could be incorporated using established methods from two-phase VE systems [Andersen, 2017, Nilsen et al., 2016b].

4 Conclusion

This study introduces and evaluates a three-phase VE modeling framework for simulation of CO_2 migration in depleted gas reservoirs, explicitly accounting for the presence of methane. The VE formulation simplifies the compositional model into a black-oil approximation and subsequently collapses the spatial domain into two dimensions with significant computational speedup.

Benchmarking across idealized and field-scale configurations shows that the model captures

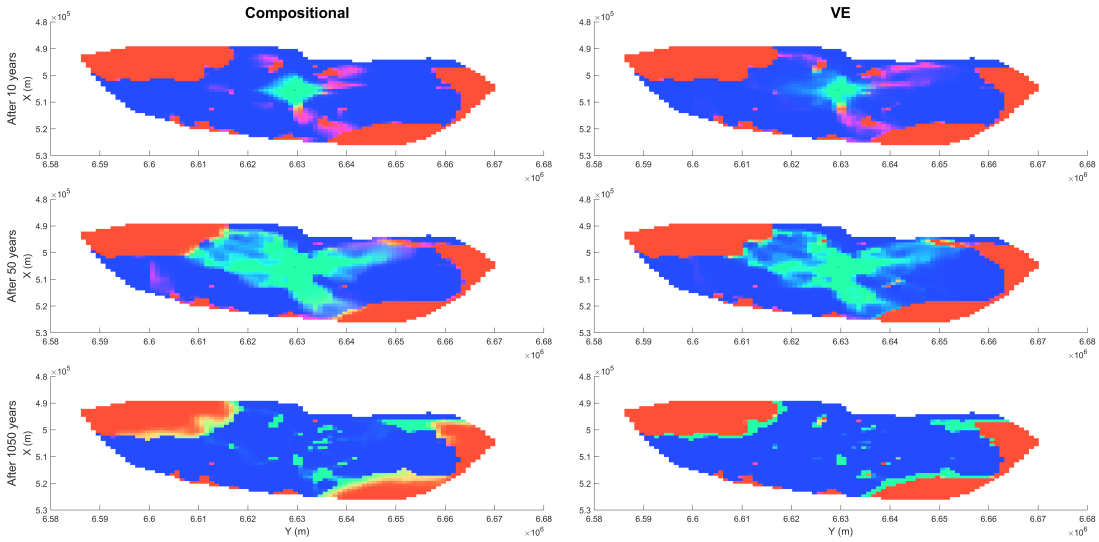

Figure 6: Case 3, Top-view comparison of CO_2 and methane plume migration after 10, 50, and 1050 years using compositional (left column) and VE (right column) models. The spatial extent of the plume is shown in the XY plane.

the key gravity-driven plume shape, lateral migration pathways, and locations of structural trapping that are most relevant for reservoir- to basin-scale assessment. Because vertical profiles are handled analytically, the formulation is largely insensitive to vertical grid refinement while coarse-grid compositional simulations are susceptible to numerical dispersion and can misrepresent the amount of fluid spilling across anticlines. Quantitatively, differences are most apparent near sharp contacts and in zones where small-scale mixing controls phase volumes, but the regional patterns and time scales of migration remain well reproduced.

Despite known limitations, the VE model delivers substantial computational gains, typically on the order of 10^2–10^3 relative to compositional models, cutting runtimes from hours or days to minutes or seconds and enabling simulations over long timeframes and large domains. This dramatic speed-up enables ensemble-centric workflows that would otherwise be impractical: rapid site screening over large geographic extents (especially valuable in early CCS project stages), systematic sensitivity studies and assessment of injection strategies, optimization under operational constraints, and workflows requiring several runs such as uncertainty quantification and history matching. For the early stages of CCS project development, where rapid screening of potential sites and assessment of various injection strategies are critical, such a tool is invaluable. While this study focused on CO_2 injection into depleted gas reservoirs, the framework is adaptable to other subsurface applications characterized by gravity segregation and extensive lateral scales, including energy storage, CO_2-enhanced gas recovery, and water-alternating-gas processes.

Open Research Section

The data associated with this manuscript will be made publicly available upon publication of the journal article.

Conflict of Interest disclosure

To the best of the authors' knowledge, there are no conflicts of interest associated with this work.

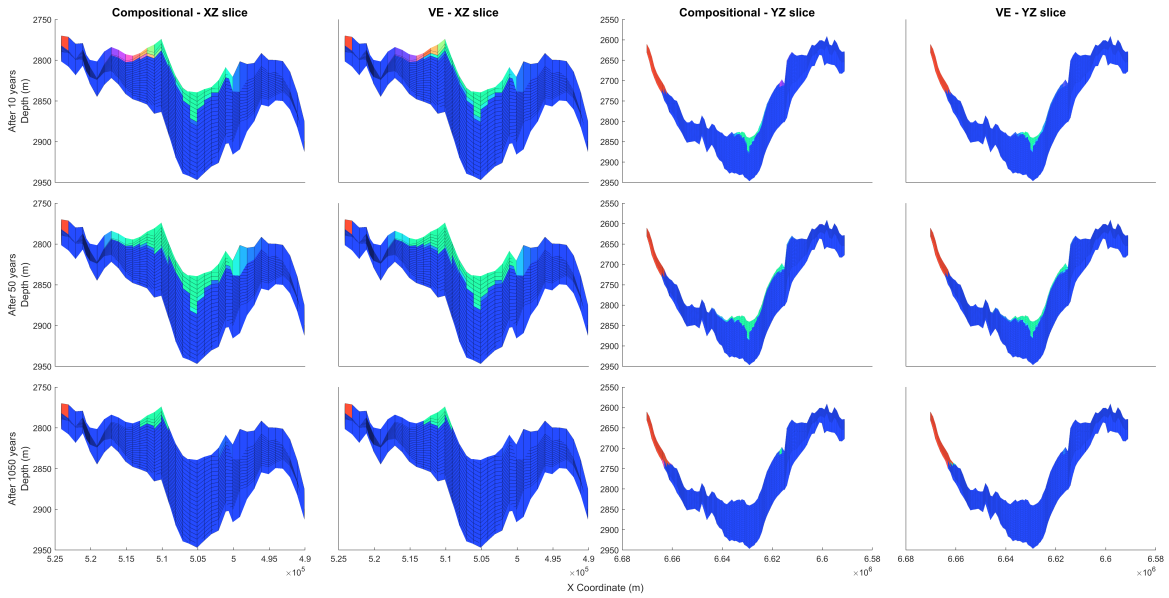

Figure 7: Case 3, Comparison of CO_2 and methane plume evolution at three time steps (10, 50, and 1050 years) for compositional and vertical equilibrium (VE) models. XZ and YZ 2D cross-sections are shown for each case.

Acknowledgments

Saeid Telvari acknowledges the support of a James Watt Scholarship from Heriot-Watt University. This work is part of the MuPSI project (Multiscale Pressure-Stress Impacts on fault integrity for multi-site regional CO_2 storage) which operates under the Clean Energy Transition Partnership (CETP).

Declaration of Generative AI Use

AI language models were used to assist with aspects of manuscript preparation. All content was reviewed, verified, and approved by the authors, who take full responsibility for the manuscript.

A Thermophysical Property Modeling of CO_2 and Methane

The density and viscosity properties of CO_2 and methane are determined through flash calculations using the equation of state across a range of pressures at 60°C. These computational results are subsequently used to develop fitted equations describing the pressure-dependent variations in density and viscosity for each component. The fitting procedure employs Fourier-type series equations with 3 to 8 terms, depending on the specific dataset characteristics. The accuracy of the fitted equations is quantified using root mean squared error analysis, as shown in Table 2. Notably, the errors associated with CO_2 are larger due to its more non-ideal behaviour compared to methane. The fitting equation takes the form:

$$f(p) = a_0 + \sum_{n=1}^{8} \left[a_n \cos(n\omega p) + b_n \sin(n\omega p) \right] \tag{36}$$

Here, $f(p)$ represents the fitted property (density or viscosity) as a function of pressure p, a_0, a_n, and b_n are fitting coefficients, ω is a frequency parameter, and n is the number of harmonic terms used, determined for each specific fluid and property being modeled.

Table 2: RMSE Errors between Fitted Equations and EoS Data

Property	CO_2	CH_4
Density	0.2137	4.1728e-05
Viscosity	2.23358e-08	2.4823e-10

Table 3: Fitted Fourier coefficients and frequency parameter (ω) for pressure-dependent property correlations

Coeff	ρ_c	ρ_m	μ_c	μ_m
a_0	4.647e+02	6.811e+01	4.717e-05	2.058e-05
a_1	-3.783e+02	-6.191e+01	-1.989e-05	-9.762e-06
b_1	-1.631e+02	1.372e+02	-2.211e-05	1.016e-06
a_2	-1.142e+02	-7.962e+00	-8.102e-06	1.302e-06
b_2	1.674e+01	-2.807e+01	-2.916e-06	7.019e-07
a_3	2.506e+00	-1.246e+00	-3.038e-06	6.118e-08
b_3	5.676e+01	2.240e+01	3.585e-06	-4.160e-07
a_4	2.021e+01	4.839e+00	-5.284e-07	–
b_4	2.251e+01	-7.902e+00	2.918e-06	–
a_5	6.303e+00	-1.827e+00	5.821e-07	–
b_5	-3.976e+00	2.764e-01	8.952e-07	–
a_6	-9.955e-01	–	5.955e-07	–
b_6	-4.553e+00	–	9.503e-09	–
a_7	-2.635e-01	–	2.104e-07	–
b_7	7.068e-01	–	-4.759e-08	–
a_8	4.358e-01	–	–	–
b_8	1.176e+00	–	–	–
ω	1.377e-07	4.909e-08	1.398e-07	6.545e-08

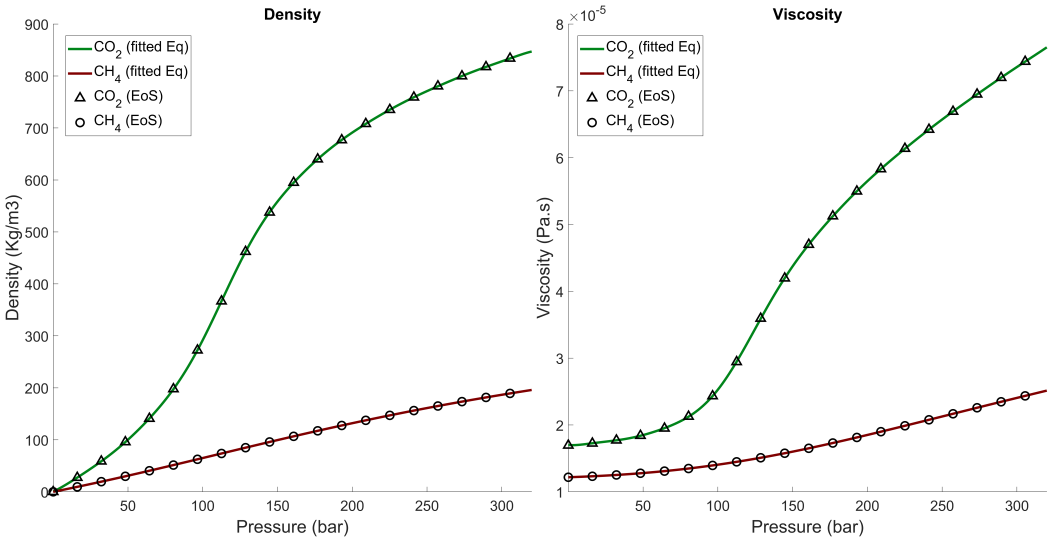

Figure 8: Density and viscosity of CO_2 and methane at T = 60°C, EoS data vs. fitted equation

References

M Ahmadinia, S M Shariatipour, O Andersen, and M Sadri. Benchmarking of vertically integrated models for the study of the impact of caprock morphology on CO₂ migration. *International Journal of Greenhouse Gas Control*, 90, 2019. ISSN 1750-5836. doi: 10.1016/j.ijggc.2019.102802. URL <GotoISI>://WOS:000495026000009.

A. Al-Hashami, S. R. Ren, and B. Tohidi. CO2 Injection for Enhanced Gas Recovery and Geo-Storage: Reservoir Simulation and Economics. 6 2005. doi: 10.2118/94129-MS. URL https://dx.doi.org/10.2118/94129-MS.

Rebecca Allen, Halvor M. Nilsen, Knut Andreas Lie, Olav Møyner, and Odd Andersen. Using simplified methods to explore the impact of parameter uncertainty on CO2 storage estimates with application to the Norwegian Continental Shelf. *International Journal of Greenhouse Gas Control*, 75:198–213, 8 2018. ISSN 17505836. doi: 10.1016/J.IJGGC.2018.05.017.

Mohammad Amin Amooie and Joachim Moortgat. Higher-order black-oil and compositional modeling of multiphase compressible flow in porous media. *International Journal of Multiphase Flow*, 105:45–59, 8 2018. ISSN 03019322. doi: 10.1016/J.IJMULTIPHASEFLOW.2018.03.016.

O. Andersen, S. E. Gasda, and H. M. Nilsen. Vertically Averaged Equations with Variable Density for CO2 Flow in Porous Media. *Transport in Porous Media*, 107:95–127, 3 2015. ISSN 15731634. doi: 10.1007/s11242-014-0427-z.

O A Andersen, H M Nilsen, and S E Gasda. Vertical Equilibrium Flow Models with Fully Coupled Geomechanics for CO2 Storage Modeling, Using Precomputed Mechanical Response Functions. *Energy Procedia*, 114:3113–3131, 2017. ISSN 1876-6102. doi: https://doi.org/10.1016/j.egypro.2017.03.1440. URL https://www.sciencedirect.com/science/article/pii/S1876610217316259.

Odd Andersen. *Simplified models for numerical simulation of geological CO2 storage*. PhD thesis, 2 2017.

Susan Anyosa, Jo Eidsvik, and Dario Grana. Evaluating geophysical monitoring strategies for a CO2 storage project. *Computers & Geosciences*, 185:105561, 3 2024. ISSN 0098-3004. doi:

10.1016/J.CAGEO.2024.105561. URL https://www.sciencedirect.com/science/article/pii/S009830042400044X.

Karl W Bandilla, Bo Guo, and Michael A Celia. A guideline for appropriate application of vertically-integrated modeling approaches for geologic carbon storage modeling. *International Journal of Greenhouse Gas Control*, 91:102808, 2019. ISSN 1750-5836. doi: https://doi.org/10.1016/j.ijggc.2019.102808. URL https://www.sciencedirect.com/science/article/pii/S1750583619300684.

Beatrix Becker, Bo Guo, Karl Bandilla, Michael A. Celia, Bernd Flemisch, and Rainer Helmig. A Pseudo-Vertical Equilibrium Model for Slow Gravity Drainage Dynamics. *Water Resources Research*, 53:10491–10507, 12 2017. ISSN 19447973. doi: 10.1002/2017WR021644.

Beatrix Becker, Bo Guo, Ivan Buntic, Bernd Flemisch, and Rainer Helmig. An Adaptive Hybrid Vertical Equilibrium/Full-Dimensional Model for Compositional Multiphase Flow. *Water Resources Research*, 58(1):e2021WR030990, 2022. ISSN 0043-1397. doi: https://doi.org/10.1029/2021WR030990. URL https://agupubs.onlinelibrary.wiley.com/doi/abs/10.1029/2021WR030990.

Tore I. Bjørnarå, Jan M. Nordbotten, and Joonsang Park. Vertically integrated models for coupled two-phase flow and geomechanics in porous media. *Water Resources Research*, 52:1398–1417, 2 2016. ISSN 19447973. doi: 10.1002/2015WR017290.

Andreas Bjørnestad, Eva Halland, and Fridtjof Riis. Evaluation of the CO2 Storage Potential of the Norwegian Continental Shelf: Online Data Repository. In *Energy Procedia*, volume 114, pages 4394–4399. Elsevier Ltd, 2017. doi: 10.1016/j.egypro.2017.03.1593.

Ivan Buntic, Martin Schneider, Bernd Flemisch, and Rainer Helmig. A fully-implicit solving approach to an adaptive multi-scale model - coupling a vertical-equilibrium and full-dimensional model for compressible, multi-phase flow in porous media. *Computational Geosciences*, 29:11, 4 2025. ISSN 1420-0597. doi: 10.1007/s10596-025-10351-z.

S Y Chen, J F Liu, Q Zhang, F Teng, and B C McLellan. A critical review on deployment planning and risk analysis of carbon capture, utilization, and storage (CCUS) toward carbon neutrality. *Renewable & Sustainable Energy Reviews*, 167, 2022. ISSN 1364-0321. doi: 10.1016/j.rser.2022.112537. URL <GotoISI>://WOS:000830429400001.

Holger Class, Anozie Ebigbo, Rainer Helmig, Helge K Dahle, Jan M Nordbotten, Michael A Celia, Pascal Audigane, Melanie Darcis, Jonathan Ennis-King, Yaqing Fan, Bernd Flemisch, Sarah E Gasda, Min Jin, Stefanie Krug, Diane Labregere, Ali Naderi Beni, Rajesh J Pawar, Adil Sbai, Sunil G Thomas, Laurent Trenty, and Lingli Wei. A benchmark study on problems related to CO2 storage in geologic formations. *Computational Geosciences*, 13(4):409–434, 2009. ISSN 1573-1499. doi: 10.1007/s10596-009-9146-x. URL https://doi.org/10.1007/s10596-009-9146-x.

B Court, K W Bandilla, M A Celia, A Janzen, M Dobossy, and J M Nordbotten. Applicability of vertical-equilibrium and sharp-interface assumptions in CO₂ sequestration modeling. *International Journal of Greenhouse Gas Control*, 10:134–147, 2012. ISSN 1750-5836. doi: 10.1016/j.ijggc.2012.04.015. URL <GotoISI>://WOS:000309790500013.

I de Jonge Anderson, H Ramachandran, U Nicholson, S Geiger, A Widyanita, and F Doster. Determining CO2 storage efficiency within a saline aquifer using reduced complexity models. *Advances in Geo-Energy Research*, 13(1):22–31, 2024. doi: 10.46690/ager.2024.07.04. URL https://www.scopus.com/inward/record.uri?eid=2-s2.0-85197686714&doi=10.46690%2fager.2024.07.04&partnerID=40&md5=b1a6413ffb543b3b9e168b67dabbacf7.

R Donat, F Guerrero, and P Mulet. Implicit-explicit methods for models for vertical equilibrium multiphase flow. *Computers & Mathematics with Applications*, 68(3):363–383, 2014. ISSN 0898-1221. doi: 10.1016/j.camwa.2014.06.006. URL <GotoISI>://WOS:000340316100020.

F. Doster, J. M. Nordbotten, and M. A. Celia. Impact of capillary hysteresis and trapping on vertically integrated models for CO2 storage. *Advances in Water Resources*, 62:465–474, 12 2013. ISSN 03091708. doi: 10.1016/j.advwatres.2013.09.005.

Florian Doster, Jan M. Nordbotten, and Michael A. Celia. Hysteretic upscaled constitutive relationships for vertically integrated porous media flow. *Computing and Visualization in Science*, 15:147–161, 8 2012. ISSN 14329360. doi: 10.1007/s00791-013-0206-3.

S E Gasda, J M Nordbotten, and M A Celia. Vertical equilibrium with sub-scale analytical methods for geological CO₂ sequestration. *Computational Geosciences*, 13(4): 469–481, 2009. ISSN 1420-0597. doi: 10.1007/s10596-009-9138-x. URL <GotoISI>://WOS:000272180000005.

S. E. Gasda, J. M. Nordbotten, and M. A. Celia. Vertically averaged approaches for CO2 migration with solubility trapping, 2011. ISSN 00431397.

Sarah E. Gasda, Halvor M. Nilsen, Helge K. Dahle, and William G. Gray. Effective models for CO2 migration in geological systems with varying topography. *Water Resources Research*, 48, 2012. ISSN 00431397. doi: 10.1029/2012WR012264.

Sarah E. Gasda, Halvor M. Nilsen, and Helge K. Dahle. Impact of structural heterogeneity on upscaled models for large-scale CO2 migration and trapping in saline aquifers. *Advances in Water Resources*, 62:520–532, 12 2013a. ISSN 03091708. doi: 10.1016/j.advwatres.2013.05.003.

Sarah E. Gasda, Elsa du Plessis, and Helge K. Dahle. Upscaled models for CO2 injection and migration in geological systems. In *Simulation of Flow in Porous Media*, pages 1–38. DE GRUYTER, 10 2013b. doi: 10.1515/9783110282245.1.

S. Ghanbari, E. J. Mackay, and G. E. Pickup. Measurement of physical dispersion in random correlated permeability fields and its application for upscaling. In *16th European Conference on the Mathematics of Oil Recovery, ECMOR 2018*. European Association of Geoscientists and Engineers, EAGE, 2018. doi: 10.3997/2214-4609.201802200.

Saeed Ghanbari, Eric J. Mackay, Niklas Heinemann, Juan Alcalde, Alan James, and Michael J. Allen. Impact of CO2 mixing with trapped hydrocarbons on CO2 storage capacity and security: A case study from the Captain aquifer (North Sea). *Applied Energy*, 278, 11 2020. ISSN 03062619. doi: 10.1016/j.apenergy.2020.115634.

F. Guerrero, R. Donat, and P. Mulet. Solving a model for 1-D, three-phase flow vertical equilibrium processes in a homogeneous porous medium by means of a Weighted Essentially Non Oscillatory numerical scheme. *Computers and Mathematics with Applications*, 66:1284–1298, 10 2013. ISSN 08981221. doi: 10.1016/j.camwa.2013.07.027.

B Guo, K W Bandilla, J M Nordbotten, M A Celia, E Keilegavlen, and F Doster. A multiscale multilayer vertically integrated model with vertical dynamics for CO₂ sequestration in layered geological formations. *Water Resources Research*, 52(8):6490–6505, 2016. ISSN 0043-1397. doi: 10.1002/2016wr018714. URL <GotoISI>://WOS:000383684400044.

Bo Guo, Karl W. Bandilla, Florian Doster, Eirik Keilegavlen, and Michael A. Celia. A vertically integrated model with vertical dynamics for CO2 storage. *Water Resources Research*, 50: 6269–6284, 8 2014. ISSN 19447973. doi: 10.1002/2013WR015215.

Bo Guo, Yiheng Tao, Karl Bandilla, and Michael Celia. Vertically Integrated Dual-porosity and Dual-permeability Models for CO2 Sequestration in Fractured Geological Formation. In *Energy Procedia*, volume 114, pages 3343–3352. Elsevier Ltd, 2017. doi: 10.1016/j.egypro.2017.03.1466.

M. Haajizadeh, F. J. Fayers, A. P. Cockin, M. Roffey, and D. J. Bond. On the Importance of Dispersion and Heterogeneity in the Compositional Simulation of Miscible Gas Processes. Society of Petroleum Engineers (SPE), 10 1999. doi: 10.2118/57264-ms.

A Hamza, I A Hussein, M J Al-Marri, M Mahmoud, R Shawabkeh, and S Aparicio. CO₂ enhanced gas recovery and sequestration in depleted gas reservoirs: A review. *Journal of Petroleum Science and Engineering*, 196, 2021. ISSN 0920-4105. doi: 10.1016/j.petrol.2020.107685. URL <GotoISI>://WOS:000600808100054.

Hassan Hassanzadeh, Mehran Pooladi-Darvish, Adel M. Elsharkawy, David W. Keith, and Yuri Leonenko. Predicting PVT data for CO2-brine mixtures for black-oil simulation of CO2 geological storage. *International Journal of Greenhouse Gas Control*, 2(1):65–77, 2008. ISSN 17505836. doi: 10.1016/S1750-5836(07)00010-2.

R. P. Hepple and S. M. Benson. Geologic storage of carbon dioxide as a climate change mitigation strategy: performance requirements and the implications of surface seepage. *Environmental Geology 2004 47:4*, 47(4):576–585, 11 2004. ISSN 1432-0495. doi: 10.1007/S00254-004-1181-2. URL https://link.springer.com/article/10.1007/s00254-004-1181-2.

Charles R Jenkins, Peter J Cook, Jonathan Ennis-King, James Undershultz, Chris Boreham, Tess Dance, Patrice de Caritat, David M Etheridge, Barry M Freifeld, Allison Hortle, Dirk Kirste, Lincoln Paterson, Roman Pevzner, Ulrike Schacht, Sandeep Sharma, Linda Stalker, and Milovan Urosevic. Safe storage and effective monitoring of CO₂ in depleted gas fields. *Proceedings of the National Academy of Sciences*, 109(2):E35–E41, 2012. doi: doi:10.1073/pnas.1107255108. URL https://www.pnas.org/doi/abs/10.1073/pnas.1107255108.

Samuel Krevor, Heleen de Coninck, Sarah E Gasda, Navraj Singh Ghaleigh, Vincent de Gooyert, Hadi Hajibeygi, Ruben Juanes, Jerome Neufeld, Jennifer J Roberts, and Floris Swennenhuis. Subsurface carbon dioxide and hydrogen storage for a sustainable energy future. *Nature Reviews Earth & Environment*, 4(2):102–118, 2023. ISSN 2662-138X. doi: 10.1038/s43017-022-00376-8. URL https://doi.org/10.1038/s43017-022-00376-8.

Ajitabh Kumar, Robin Ozah, Myeong Noh, Gary A. Pope, Steven Bryant, Kamy Sepehmoori, and Larry W. Lake. Reservoir Simulation of CO2 Storage in Deep Saline Aquifers. *SPE Journal*, 10(03):336–348, 9 2005. ISSN 1086-055X. doi: 10.2118/89343-PA. URL https://dx.doi.org/10.2118/89343-PA.

H C Lau, S Ramakrishna, K Zhang, and A V Radhamani. The Role of Carbon Capture and Storage in the Energy Transition. *Energy & Fuels*, 35(9):7364–7386, 2021. ISSN 0887-0624. doi: 10.1021/acs.energyfuels.1c00032. URL <GotoISI>://WOS:000648878900028.

Knut-Andreas Lie. *An Introduction to Reservoir Simulation Using MATLAB/GNU Octave: User Guide for the MATLAB Reservoir Simulation Toolbox (MRST)*. Cambridge University Press, Cambridge, 2019. ISBN 9781108492430. doi: DOI:10.1017/9781108591416. URL https://www.cambridge.org/core/product/F48C3D8C88A3F67E4D97D4E16970F894.

Knut-Andreas Lie and Olav Møyner. *Advanced Modeling with the MATLAB Reservoir Simulation Toolbox*. Cambridge University Press, Cambridge, 2021. ISBN 9781316519967. doi: DOI:10.1017/9781009019781. URL https://www.cambridge.org/core/product/7AC2425C73F6F729DB88DB1A504FA1E7.

Shezhan Liu, Lei Yuan, Changzhong Zhao, Yi Zhang, and Yongchen Song. A review of research on the dispersion process and CO2 enhanced natural gas recovery in depleted gas reservoir, 1 2022. ISSN 09204105.

Jianli Ma, Qi Li, Thomas Kempka, and Michael Kühn. Hydromechanical Response and Impact of Gas Mixing Behavior in Subsurface CH4 Storage with CO2-Based Cushion Gas. *Energy & Fuels*, 33(7):6527–6541, 7 2019. ISSN 0887-0624. doi: 10.1021/acs.energyfuels.9b00518. URL https://doi.org/10.1021/acs.energyfuels.9b00518.

Rafael March Castaneda Neto. Modelling of CO2 storage in naturally fractured reservoirs, 2018. URL http://hdl.handle.net/10399/3516.

Carlos Méndez, Nicholas Simpson, Francis Johnson, and Arlene Birt. *Climate Change 2023: Synthesis Report (Full Volume) Contribution of Working Groups I, II and III to the Sixth Assessment Report of the Intergovernmental Panel on Climate Change*. 7 2023. doi: 10.59327/IPCC/AR6-9789291691647.

O. Moyner. JutulDarcy.jl - a Fully Differentiable High-Performance Reservoir Simulator based on Automatic Differentiation. In *ECMOR 2024*, volume 2024, pages 1–37. European Association of Geoscientists & Engineers, 9 2024. doi: 10.3997/2214-4609.202437111. URL https://www.earthdoc.org/content/papers/10.3997/2214-4609.202437111.

O Moyner and H M Nilsen. Multiresolution coupled vertical equilibrium model for fast flexible simulation of CO₂ storage. *Computational Geosciences*, 23(1):1–20, 2019. ISSN 1420-0597. doi: 10.1007/s10596-018-9775-z. URL <GotoISI>://WOS:000459423400001.

N S Muhammed, M B Haq, D A Al Shehri, A Al-Ahmed, M M Rahman, E Zaman, and S Iglauer. Hydrogen storage in depleted gas reservoirs: A comprehensive review. *FUEL*, 337, 2023. ISSN 0016-2361. doi: 10.1016/j.fuel.2022.127032.

Trine S. Mykkeltvedt and Jan M. Nordbotten. Estimating effective rates of convective mixing from commercial-scale injection. *Environmental Earth Sciences*, 67:527–535, 9 2012. ISSN 18666280. doi: 10.1007/s12665-012-1674-3.

H M Nilsen, K A Lie, and O Andersen. Fully-implicit simulation of vertical-equilibrium models with hysteresis and capillary fringe. *Computational Geosciences*, 20(1):49–67, 2016a. ISSN 1420-0597. doi: 10.1007/s10596-015-9547-y. URL <GotoISI>://WOS:000373347600004.

H M Nilsen, K A Lie, and O Andersen. Robust simulation of sharp-interface models for fast estimation of CO₂ trapping capacity in large-scale aquifer systems. *Computational Geosciences*, 20(1):93–113, 2016b. ISSN 1420-0597. doi: 10.1007/s10596-015-9549-9. URL <GotoISI>://WOS:000373347600006.

J. M. Nordbotten and H. K. Dahle. Impact of the capillary fringe in vertically integrated models for CO 2 storage. *Water Resources Research*, 47, 2011. ISSN 00431397. doi: 10.1029/2009WR008958.

Jan Nordbotten and Michael Celia. Geological Storage of CO: Modeling Approaches for Large-Scale Simulation. *Geological Storage of CO2: Modeling Approaches for Large-Scale Simulation*, pages i–ix, 11 2011. ISSN 9780470889466. doi: 10.1002/9781118137086.fmatter.

C M Oldenburg, K Pruess, and S M Benson. Process Modeling of CO2 Injection into Natural Gas Reservoirs for Carbon Sequestration and Enhanced Gas Recovery. *Energy & Fuels*, 15(2):293–298, 3 2001. ISSN 0887-0624. doi: 10.1021/ef000247h. URL https://doi.org/10.1021/ef000247h.

Curtis M Oldenburg and Escholarship Org. Carbon sequestration in natural gas reservoirs: enhanced gas recovery and natural gas storage. 2003. URL https://escholarship.org/content/qt61b1p0gk/qt61b1p0gk.pdf.

Milan J Patel, Eric F May, and Michael L Johns. High-fidelity reservoir simulations of enhanced gas recovery with supercritical CO2. *Energy*, 111:548–559, 2016. ISSN 0360-5442. doi: https://doi.org/10.1016/j.energy.2016.04.120. URL https://www.sciencedirect.com/science/article/pii/S0360544216305400.

Per Pettersson, Svenn Tveit, and Sarah E. Gasda. Dynamic estimates of extreme-case CO2 storage capacity for basin-scale heterogeneous systems under geological uncertainty. *International Journal of Greenhouse Gas Control*, 116:103613, 5 2022. ISSN 1750-5836. doi: 10.1016/J.IJGGC.2022.103613. URL https://www.sciencedirect.com/science/article/pii/S1750583622000329.

Hariharan Ramachandran, Iain de Jonge-Anderson, Ikhwanul Hafizi Musa, Uisdean Nicholson, Chee Phuat Tan, Sebastian Geiger, and Florian Doster. Rapid Fault Leakage Modeling for CO2 Storage in Saline Aquifers. 8 2024. doi: 10.31223/X5S12N. URL https://eartharxiv.org/repository/view/7535/.

Philip S. Ringrose, Anne Kari Furre, Stuart M.V. Gilfillan, Samuel Krevor, Martin Landroslash, Rory Leslie, Tip Meckel, Bamshad Nazarian, and Adeel Zahid. Storage of Carbon Dioxide in Saline Aquifers: Physicochemical Processes, Key Constraints, and Scale-Up Potential. *Annual Review of Chemical and Biomolecular Engineering*, 12:471–494, 6 2021. ISSN 19475446. doi: 10.1146/ANNUREV-CHEMBIOENG-093020-091447,. URL https://pubmed.ncbi.nlm.nih.gov/33872518/.

Lorenzo Rosa and Marco Mazzotti. Potential for hydrogen production from sustainable biomass with carbon capture and storage. *Renewable and Sustainable Energy Reviews*, 157:112123, 2022. ISSN 1364-0321. doi: https://doi.org/10.1016/j.rser.2022.112123. URL https://www.sciencedirect.com/science/article/pii/S136403212200051X.

Vijay Kumar Shrivastava. Physical Dispersion in Compositional Reservoir Simulation. Technical report, 2003. URL http://hdl.handle.net/1880/39841.

Amine Tadjer, Aojie Hong, and Reidar B. Bratvold. A sequential decision and data analytics framework for maximizing value and reliability of CO2 storage monitoring. *Journal of Natural Gas Science and Engineering*, 96:104298, 12 2021. ISSN 1875-5100. doi: 10.1016/J.JNGSE.2021.104298. URL https://www.sciencedirect.com/science/article/pii/S1875510021004959.

Yiheng Tao, Bo Guo, Karl W. Bandilla, and Michael A. Celia. Vertically integrated dual-continuum models for CO2 injection in fractured geological formations. *Computational Geosciences*, 23:273–284, 4 2019. ISSN 15731499. doi: 10.1007/s10596-018-9805-x.

George A. Virnovsky, Hans Martin Helset, and Svein M. Skjæveland. Stability of displacement fronts in WAG operations. *SPE Journal*, 1:383–393, 1996. ISSN 1086055X. doi: 10.2118/28622-pa.

Christopher J. Wareing, Michael Fairweather, Samuel A.E.G. Falle, and Robert M. Woolley. Validation of a model of gas and dense phase CO2 jet releases for carbon capture and storage application. *International Journal of Greenhouse Gas Control*, 20:254–271, 2014. ISSN 17505836. doi: 10.1016/j.ijggc.2013.11.012.

B Wei, B W Wang, X Li, M Aishan, and Y Ju. CO₂ storage in depleted oil and gas reservoirs: A review. *Advances in Geo-Energy Research*, 9(2):76–93, 2023. ISSN 2207-9963. doi: 10.46690/ager.2023.08.02. URL <GotoISI>://WOS:001054316800002.

Tianyuan Zheng, Bo Guo, and Haibing Shao. A hybrid multiscale framework coupling multilayer dynamic reconstruction and full-dimensional models for CO2 storage in deep saline aquifers. *Journal of Hydrology*, 600, 9 2021. ISSN 00221694. doi: 10.1016/j.jhydrol.2021.126649.